Applied Surface Science 554 (2021) 149311

Contents lists available at ScienceDirect

Applied Surface Science

journal homepage: www.elsevier.com/locate/apsusc

Full Length Article

Unveiling the anisotropic behavior of ultrafast electron transfer at the metal/organic interface

Fernando Aguilar-Galindo [a,b], Andrey G. Borisov [c], Sergio Díaz-Tendero [a,d,e,*]

[a] Departmento de Química, Módulo 13, Universidad Autónoma de Madrid, 28049 Madrid, Spain
[b] Donostia International Physics Center (DIPC), Paseo Manuel de Lardizabal 4, Donostia-San Sebastián E-20018, Spain
[c] Institut des Sciences Moléculaires d'Orsay – UMR 8214, CNRS, Université Paris Saclay, 91405 Orsay, France
[d] Condensed Matter Physics Center (IFIMAC), Universidad Autónoma de Madrid, 28049 Madrid, Spain
[e] Institute for Advanced Research in Chemical Science (IAdChem), Universidad Autónoma de Madrid, 28049 Madrid, Spain

ARTICLE INFO

Keywords:
Molecular adsorption
Wave packet propagation
Ultrafast electron dynamics
Surface electronic structure
Organic/metal interfaces

ABSTRACT

Ultrafast electron transfer between adsorbed organic molecules and metal substrates is studied. In particular, the dynamics of the active electron in the nitroethylene anion/metal-copper surface system has been followed in real time using a wave packet propagation approach, allowing a rigorous analysis of the decay of molecule-localized electronic resonances. We find that the strong coupling with the metal substrate leads to an extremely short lifetime (∼ 1fs) of the π^* molecular resonance. Comparison between the free-electron metal, Cu(1 0 0), and Cu (1 1 1) surfaces demonstrates that the electronic band structure of the substrate and the shape of the decaying molecular orbital lead to a highly marked anisotropy of the metal continuum states populated by resonant electron transfer from the adsorbate. This finding points at possible anisotropy effects in adsorbate–adsorbate interactions and it is of particular importance in molecular self assembly at metal surfaces, thus opening the way to a rational design of hybrid metal/organic interfaces with tailored electronic properties.

1. Introduction

Single particle experiments are not a chimera anymore and today state-of-the-art techniques can be used for the detection, manipulation, and properties' analysis of individual quantum objects [1–6]. Among the different techniques to study properties of a single molecule adsorbed on a substrate, Scanning Tunneling Microscopy (STM) [7,8] is a particular versatile method that provides an atomic-scale probe and which can be used to reveal electron densities of molecular orbitals [9,10], as well as to control the charge state of an adsorbate [11,12], or to visualize bond formation between atoms and organic molecules [13]. Moreover, energies and lifetimes of decaying quasi-stationary electronic states of individual molecules and nanostructures adsorbed on metal surfaces can be determined with Scanning Tunneling Spectroscopy (STS) [14,15]. This information is nicely completed by Time-Resolved Two-Photon-Photoemission (TR-2PPE) studies of the dynamics of excited states at pristine and adsorbate coated surfaces [16–20]. It is worth mentioning that, along with STM, other proximal probe imaging techniques, such as Atomic Force Microscopy (AFM) with functionalized tips [21], are quite efficient and several properties of individual molecules can be resolved atomically such as charge distribution [22], bond order [23], and adsorption geometry [24]. Recently, a step forward in single-molecule experiments has taken place with the development of techniques in which an Ångstrom scale precise electron injection with an STM tip induces excitation of a single molecule. Thus, atomic scale resolved maps of vibrational excitation [25–29], reactivity [13,30–33], and photon emission [34–38] are obtained.

Many of the phenomena of current interest involve initially empty electronic orbitals of the adsorbed molecules populated either by an excitation with photons or electrons (in this situation a molecular exciton can be produced), or by the direct injection of the electrons from the substrate or from an STM tip forming a molecular anion [29,37,39–43]. Creation of such an excited state can e.g. lead to photon emission (luminescence at surfaces), or can trigger nuclear dynamics leading to specific chemical reactions (surface reactivity). Other experimental techniques based on optical emission spectroscopy have been proposed to analyze the structure of molecular monolayers adsorbed on metal surfaces [44,45], imaging molecular adsorption and desorption dynamics on graphene [46], or ultra-sensitive surface spectroscopy of molecules deposited on optical nanofibers [47].

* Corresponding author at: Departmento de Química, Módulo 13, Universidad Autónoma de Madrid, 28049 Madrid, Spain.
E-mail address: sergio.diaztendero@uam.es (S. Díaz-Tendero).

https://doi.org/10.1016/j.apsusc.2021.149311
Received 27 November 2020; Received in revised form 22 January 2021; Accepted 10 February 2021
Available online 10 March 2021

However, for molecules adsorbed at metal surfaces, the coupling between the adsorbate-localized electronic states and the continuum of electronic states of metal leads to the de-excitation of the molecule-localized excited state via one-electron energy-conserving transfer from the molecular orbital into the metal (resonant electron transfer, RET), or via multi-electron relaxation [39–43,48,49]. Usually these processes are extremely efficient resulting in a lifetime of the excited state on the femtosecond (fs) time scale. The too short lifetime of an excited state harms the luminescence or surface reactivity, which evolve at much longer characteristic times, on the picosecond (ps) and even nanosecond (ns) timescales. It is then of paramount importance to understand the excited state decay, and in particular the RET as the most efficient mechanism because of its one-electron nature.

This is precisely the goal of the present work: to understand the ultrafast dynamics of RET from an adsorbed molecular anion into a metal substrate. To this end we have chosen nitroethylene interacting with a free electron metal, Cu(1 0 0), and Cu(1 1 1) surfaces, characterized by their very different electronic structure. We show that a strong coupling with the metal surface turns the molecule-localized π^* orbital into a resonance with fs lifetime, and that many characteristics of the RET can be understood as resulting from the surface projected band structure. Even if this finding is inline with earlier reports for atomic adsorbates [48–53], we demonstrate here that the decay of the molecule-localized resonance is a much more complex process. The arrangement of the atoms within the molecule, and the electronic properties of the molecule–metal interface lead to specific decay characteristics, with pronounced anisotropy of the hot electron distribution in the metal resulting from the decay of the molecular π^* resonance. Our finding is of particular relevance for such an active area of surface science as surface-supported organic networks. The strong anisotropy in the adsorbate/substrate electronic coupling is of importance for their electronic properties [54–57], and for their structural properties, which depend on indirect adsorbate–adsorbate interactions with the substrate [58–60]. The results reported here are also of interest for engineering the surface electronic structure, where the electronic surface state of the substrate is confined using organic adsorbates [61–64].

2. Results and discussion

We first present the results obtained for the adsorption of nitroethylene on the Cu(1 0 0) and Cu(1 1 1) surfaces (see Fig. 1). We observe two main surface-molecule binding sites, through the vinyl and the nitro groups. In the Cu(1 0 0) surface, a direct bond is formed between the vinyl group and one Cu atom of the surface; and a second interaction is observed with the dipole localized on the nitro group polarizing the electron cloud in the surface. A similar situation can be appreciated in the Cu(1 1 1) surface; however, in this case the metal deformation is larger with a Cu atom lifted out of the surface plane. It is precisely the surface Cu atom that directly interacts with the terminal C atom of the vinyl group. The molecule also experiences different deformations at both surfaces: while in Cu(1 1 1) the nitro group remains in the molecular plane, in the case of Cu(1 0 0) the oxygen atoms of this group are slightly out of the molecular plane pointing towards the metal.

Vinyl group as anchoring point to metal surfaces has been previously observed in acrylamide, acrylonitrile and acrolein interacting with Cu (1 0 0) and Cu(1 1 1) surfaces [65,66]. In these cases, molecule–metal interactions have been explained with a simple chemical picture: donation from the occupied lone pair and π orbitals of the molecule to the surface and backdonation from the surface to the π^* orbital of the molecule (π–backbonding). In the nitroethylene case, we have also analyzed the charge transfer upon adsorption between the molecule and the surface. Fig. 1 also shows the density difference plots ($\Delta\rho$): electron density redistribution, gain and depletion of electrons, induced by the adsorption of the molecule on the surface. From these plots a similar conclusion can be extracted: strong metal–molecule interactions are driven through the π and π^* orbitals of the molecule in a cooperative donation–backdonation manner.

The electronic structure of anionic nitroethylene is characterized by a very high electron affinity leading to a strongly bound anion state; For the free-standing molecule in vacuum the electron affinity is $E_a = -108$ meV, computed at the CCSD/cc-pVDZ//MP2/cc-pVDZ level of theory [67]. For typical metals the external π^* orbital of the nitroethylene anion has an energy above the Fermi level of the metal and well below the vacuum level. Moreover, it falls energetically into the projected band gap of nobel metal surfaces such as Cu(1 0 0) (*X*-gap) and Cu(1 1 1) (*L*-gap), where an electron propagation inside metal in the direction perpendicular to the surface is impossible within a certain energy range [68–71]. Thus, we considered nitroethylene absorbed on a Cu surface as a representative system to study the role of the substrate band structure in the RET decay of π^* molecular resonances at metal surfaces. For the sake of comparison, we have also studied the decay of the anion localized resonance in the case of the same molecule adsorbed on a free-electron *jellium* metal surface [72,73].

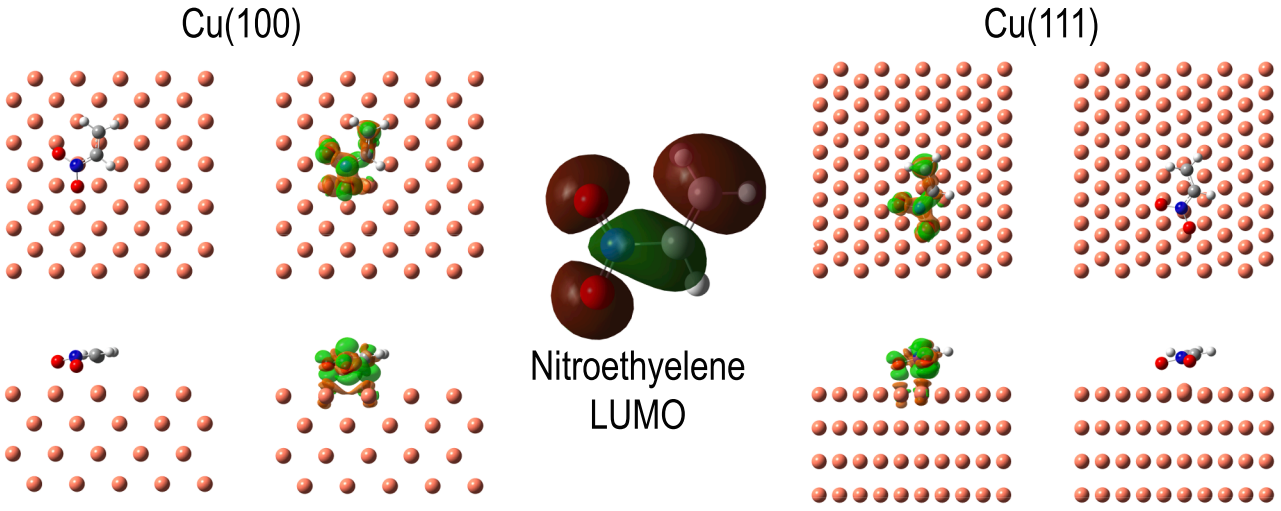

Fig. 1. Optimized geometry of nitroethylene absorbed on Cu(1 0 0) and Cu(1 1 1). The atomic color code is Cu–orange, C–grey, H–white, O–red, N–blue. All the atoms in the cell employed in the DFT simulations are shown. Change in the electronic density upon adsorption is also shown, $\Delta\rho$ (isovalue = 0.025) – green lobes show positive $\Delta\rho$, and red lobes show negative $\Delta\rho$. π^* state of nitroethylene in the gas phase is shown for comparison (isovalue = 0.02). (For interpretation of the references to colour in this figure legend, the reader is referred to the web version of this article.)

The results for the energy E_r, decay rate Γ_r, and lifetime $\tau_r = 1/\Gamma_r$ of the molecular anion resonance associated with π^* orbital of nitroethylene adsorbed on Cu(1 0 0), Cu(1 1 1), and free-electron *jellium* metal surfaces are summarized in Table 1. See section Methods, where we detail the procedure to extract these values. We remark at this point that for the *jellium* metal surface we used the potentials in the adsorption region identical to those calculated for the Cu(1 0 0) case. The only difference between the two situations is the free-electron character of the metal continuum for the *jellium* case. Comparison between the anion resonance characteristics obtained for the considered surfaces shows that, because of the different absorption geometries and associated changes in the chemical bonding, the negative ion resonance is less bound on the Cu(1 1 1) surface. The decay of the π^* resonance population via the RET into the continuum of the electronic states of the metal is fastest for the *jellium* surface resulting in the shortest lifetime of the π^* resonance in the three studied cases. The most stable anion is obtained for the absorption on Cu(1 0 0) surface. At this point, we conjecture that the difference in the resonance lifetimes results from the role of the projected band electronic structure of the metal, determining the decay dynamics of the molecule-localized state.

The differences in the molecular anion decay at free-electron, Cu (1 0 0), and Cu(1 1 1) metal surfaces are emphasized with Fig. 2, where we show the electron density corresponding to the wave function of the molecule-localized π^* resonance, calculated with the Wave-Packet Propagation (WPP) method, for the nitroethylene molecule adsorbed on these surfaces. The results are presented in the plane perpendicular to the metal surface. The orientation of the image plane with respect to the molecule is shown with arrows in the inserts. The resonant wave function contains the contribution (i) of the molecule-localized state, and (ii) of the metal continuum states populated by RET. This latter appears as an outgoing electron flux from the molecule-localized π^* resonance into the substrate, and it reflects the corresponding hot electron distribution inside the metal.

In the case of the free-electron *jellium* metal surface, the electron flux propagating towards the metal bulk is oriented close to the surface normal. I.e. an electron escapes from the molecule localized orbital into the metal continuum along the surface normal which corresponds to the shortest distance separating the molecular potential well from the metal potential well. This is in sheer contrast with the results obtained for the Cu(1 0 0) and Cu(1 1 1) surfaces, where the flux of outgoing electrons inside metal appears at a finite angle with respect to the z-axis and the oscillating structure of the electron density reflects the arrangement of atomic planes inside metal. Note also that for the Cu(1 1 1) surface part of the outgoing electron flux is oriented parallel to the surface.

In order to understand the dependence of the π^* resonance decay on the substrate we show in Fig. 3 the energy dispersion of the electronic states relevant for RET between an adsorbed molecule and the metal. Energies of the states are shown as a function of the electron momentum parallel to the surface, $\vec{k}_\parallel$. For the 1D model potential used here [74] (see Methods), the energy dispersion of the metal states with $\vec{k}_\parallel$ is given by the free electron parabola $E = E^{\bar{\Gamma}} + k_\parallel^2/2$, where $k_\parallel = \left|\vec{k}_\parallel\right|$, and the energies at the $\bar{\Gamma}$ point, $E^{\bar{\Gamma}}$, are given in Table 2. The molecule-localized state is non-dispersive and appears at constant energy.

Table 1
Energy (E_r) measured from the vacuum level, width (Γ_r), and lifetime (τ_r) of the anion π^* resonance for the nitroethylene molecule adsorbed on the three different models for the metal surface.

	Cu(1 0 0)	Cu(1 1 1)	*jellium*
E_r (eV)	−1.656	−1.024	−1.421
Γ_r (eV)	0.37	0.46	0.59
τ_r (fs)	1.78	1.43	1.12

For the Cu(1 0 0) and Cu(1 1 1) surfaces at $k_\parallel = 0$ there is no electronic states of the metal in energy resonance with the π^* orbital. Thus, the projected band gap blocks the molecule-surface RET along the surface normal. For the *jellium* metal the projected band gap is absent, all the states above the valence band (VB) bottom are then available for electronic transitions provided $k_\parallel \leqslant k_m$. This is consistent with the shortest lifetime of the π^* resonance in this case. Using the parabolic dispersion of the metal continuum states with $\vec{k}_\parallel, k_m$ can be obtained from $k_m = \sqrt{2(E_r - E_{VB}^{\bar{\Gamma}})}$. For the energy of the bottom of the metal valence band at the $\bar{\Gamma}$ point, $E_{VB}^{\bar{\Gamma}}$ of the model jellium metal surface we use the same value as that for Cu(1 1 1) and Cu(1 0 0). From the data in Table 1 and Table 2 we obtain that $k_m = 0.88$ a.u. in this case.

According to the energy dispersion analysis in Fig. 3, the decay of the π^* orbital population of the nitroethylene anion adsorbed on Cu(1 0 0) and Cu(1 1 1) surfaces is only possible by RET into the substrate states propagating at some angle with respect to the surface normal, at finite $k_\parallel$ within the range $k_b \leqslant k_\parallel \leqslant k_m$. Here k_b can be obtained from $k_b = \sqrt{2(E_r - E_{X,b}^{\bar{\Gamma}})}$ and $k_b = \sqrt{2(E_r - E_{L,b}^{\bar{\Gamma}})}$ for Cu(1 0 0) and Cu(1 1 1) surfaces respectively. Here, $E_{X,b}^{\bar{\Gamma}}$ and $E_{L,b}^{\bar{\Gamma}}$ are the energies of the bottom of the projected band gap at the $\bar{\Gamma}$ point (X-gap for Cu(100) and L-gap for Cu (111)). From the data in Table 1 and Table 2 we obtain that the threshold for the transitions into the bulk states is at $k_b = 0.32[0.59]$ a.u., and the maximum possible momentum parallel to the surface is $k_m = 0.87[0.9]$ a.u. for Cu(1 0 0) [Cu(1 1 1)]. For a given energy, the valence band states with higher $k_\parallel$ are less protruding from the metal surface into the vacuum, and thus are less coupled with molecular localized states. One then expects that RET from the molecule-localized resonance into the metal is dominated by the valence band states with $k_\parallel = 0$ in the case of the *jellium* metal. For Cu(1 0 0) and Cu(1 1 1) RET into the bulk is dominated by the valence band states wth $k_\parallel \sim k_b$, resulting in a well defined polar angle between the surface normal and the outgoing electron flux. This explains the angle dependence of the results shown in Fig. 2. The projected band gap effect was also reported for atomic adsorbates [49]. However, our results demonstrate that RET at the molecule/metal interface is much more complex with not only polar but also with pronounced azimuthal dependence of the decay.

Interestingly, since the π^* resonance is closer to the edge of the projected band gap of Cu(1 0 0) surface (k_b is smaller for Cu(1 0 0) than for Cu(1 1 1)) one expects the RET to be faster in this latter case. However, the WPP results show the inverse trend. The reason for this apparent controversy consists in the contribution of the surface state continuum to the anion decay. Absent in the projected band gap of Cu (1 0 0), the surface state within the projected band gap of Cu(1 1 1) corresponds to an electron trapped at the metal vacuum interface and moving quasi-freely parallel to the surface [75]. The wave function of the Cu(1 1 1) surface state reaches its maximum close to the surface atomic layer and exponentially decays into the metal bulk, as shown in the insert of Fig. 3b. Due to the surface localization of this state, it is strongly coupled with the π^* orbital of the adsorbed molecule and represents an extremely efficient decay channel of the molecule-localized resonance, also observed for atomic species [49,76]. The corresponding panel of Fig. 2 nicely illustrates the decay of the molecular localized state into the surface state continuum with an outgoing electron flux moving parallel to the surface with finite momentum $k_\parallel = k_S$, where $k_S = \sqrt{2(E_r - E_S^{\bar{\Gamma}})} = 0.563$ a.u. as can be obtained using Table 1 and Table 2.

Prior to further discussion of the WPP results let us consider predictions of the perturbative Bardeen Transfer Hamiltonian Theory [77–79] (see Methods), largely used in the context of electron tunneling at surfaces [80–82]. The transition matrix elements, $\mathscr{T}_{\vec{k}_\parallel, E_r}$, describe RET between the molecule-localized state metal continuum states

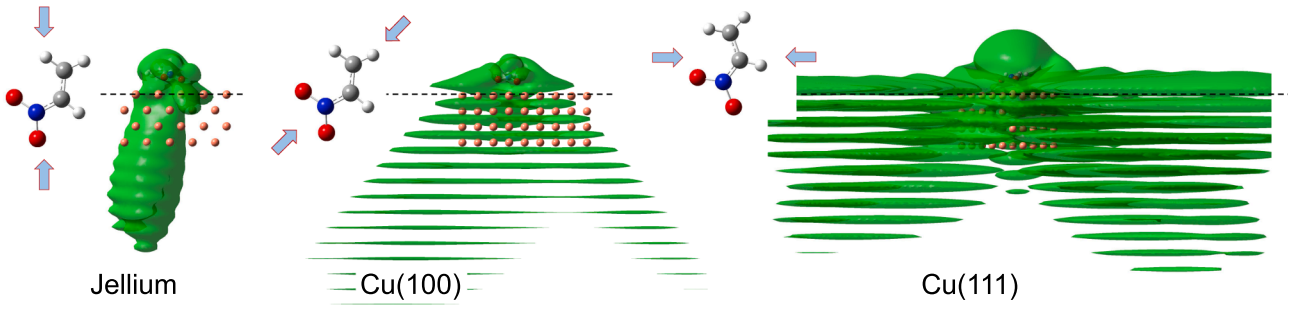

Fig. 2. Top view with the geometry of the molecule adsorbed at the surface (oxygen atoms are shown with red balls, nitrogen-blue, carbon-gray, and hydrogen-white), and the lateral view of the resonant wave function. The lateral view represents the electron density in the plane perpendicular to the surface. The arrows in the insets with the top view of the molecular structure, define the intersection line between the plane of the surface and the perpendicular plane chosen to display the electron density. The electron densities are calculated with wave packet propagation method for the nitroethylene molecular anion adsorbed on (i) a free electron surface – *jellium* model (left panel, isovalue 0.005 a.u.), (ii) a Cu(1 0 0) surface (central panel, isovalue 0.005 a.u.), and (iii) a Cu(1 1 1) surface (right panel, isovalue 0.001 a.u.). The optimal isovalues were chosen in each case to visualize the decay of the molecular localized resonance, and to ease the discussion of the underlying physics. The dashed line indicates the position of the surface plane of Cu atoms (orange balls). (For interpretation of the references to colour in this figure legend, the reader is referred to the web version of this article.)

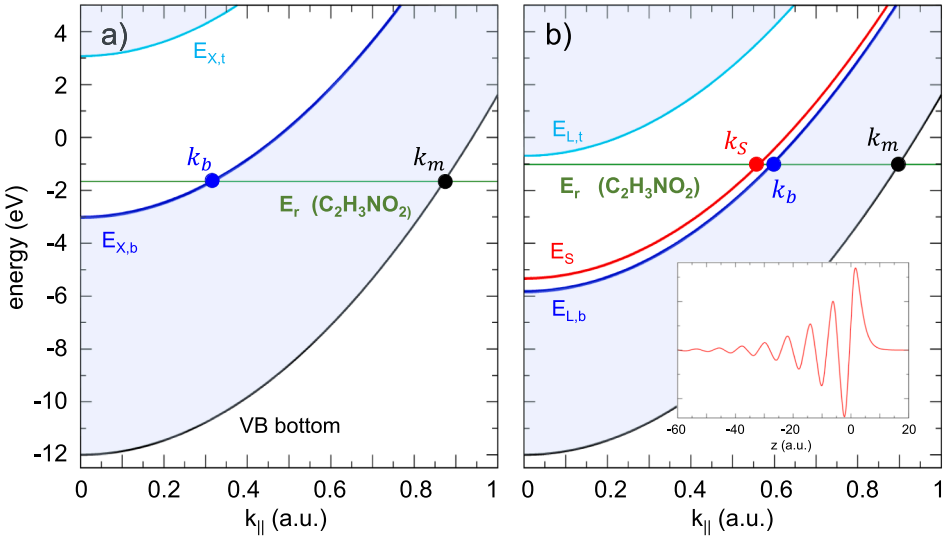

Fig. 3. Dispersion of the electronic states relevant for the decay of the nitroethylene anion adsorbed on (a) Cu(1 0 0), and (b) Cu(1 1 1) surfaces. The energy of the states is shown as a function of the electron momentum parallel to the surface $k_{||}$. Shaded region: metal continuum states available for RET. Black line, VB: valence band bottom. Blue lines, $E_{X,b}$ and $E_{L,b}$: bottom of the corresponding projected band gap. Cyan lines, $E_{X,t}$ and $E_{L,t}$: top of the corresponding projected band gap. Symbols *X* and *L* stand for the X-gap of Cu(1 0 0) and L-gap of Cu(1 1 1). Red line, E_S: surface state of Cu(1 1 1). Horizontal green line, E_r: non-dispersive molecular resonance (values in Table 1). The insert in panel (b) shows the wave function of the surface state at the Cu (1 1 1) surface, where the *z*-coordinate perpendicular to the surface is measured from the topmost layer of surface atoms. For further details see the main text. (For interpretation of the references to colour in this figure legend, the reader is referred to the web version of this article.)

Table 2
Energies in electronvolts (eV) of the metal states relevant for the RET between molecular anion and the surface. The energies with respect to the vacuum level are given at the $\bar{\Gamma}$ point i.e. for $k_{||}$=0. VB stands for the valence band, and SS stands for the surface state. $E^{\bar{\Gamma}}_{X,b}$, $E^{\bar{\Gamma}}_{L,b}$ ($E^{\bar{\Gamma}}_{X,t}$, $E^{\bar{\Gamma}}_{L,t}$) is the energy of the bottom (top) of the *X*-gap of Cu(100) and *L*-gap of Cu(111) surface. $E^{\bar{\Gamma}}_{VB}$ is the energy of the valence band bottom, and $E^{\bar{\Gamma}}_{S}$ is the energy of the surface state.

	X-gap $E^{\bar{\Gamma}}_{X,b}\rightarrow E^{\bar{\Gamma}}_{X,t}$	*L*-gap $E^{\bar{\Gamma}}_{L,b}\rightarrow E^{\bar{\Gamma}}_{L,t}$	VB $E^{\bar{\Gamma}}_{VB}$	SS $E^{\bar{\Gamma}}_{S}$
Cu(1 0 0)	−3.02 → + 3.08		−12	
Cu(1 1 1)		−5.83 → −0.69	−12	−5.33

defined by total energy E_r and electron momentum parallel to the surface $\vec{k}_{||} = (k_x, k_y)$. Thus, $\left|\mathscr{T}_{\vec{k}_{||},E_r}\right|^2$ provides the $\vec{k}_{||}$ distribution of the hot electron injected into the metal by the decaying resonance. Following the Transfer Hamiltonian Theory, $\mathscr{T}_{\vec{k}_{||},E_r}$ reflects the 2D Fourier transform, $\mathscr{F}(k_x, k_y, z_0)$, of the molecular orbital in the (x,y) plane parallel to the surface and located at a given z_0 with respect to the tunneling barrier. In Fig. 4a we show the Fourier spectrum $\left|\mathscr{F}(k_x, k_y, z_0)\right|^2$ of the π^* orbital of the free-standing nitroethylene molecule; z_0 is set 2 a.u. below the oxygen atom that appears closest to the surface for an adsorbed molecule. The atomic arrangement used for the molecule corresponds to the adsorption geometry obtained for the Cu(1 0 0) and Cu(1 1 1) surfaces. Along with the bright spot centered at $k_{||} = 0$, one observes four spots at finite $k_{||}$ reflecting the orientation of the positive lobes of the π^* orbital.

In the present WPP study a detailed analysis of the distribution of the hot electrons injected into the metal by the decaying π^* resonance is performed using a "virtual detector", located in the (x,y) plane, parallel to the metal surface. The detector is positioned at $z = z_d$ deep enough inside metal in the asymptotic region where the adsorbate induced potential is completely screened, and an outgoing electron moves under the action of the metal potential only. Typically we place the detector ~ 30 a.u. below the outermost layer of metal atoms. The results obtained using the "virtual detector" technique are summarized in Fig. 4b,c.

In Fig. 4b we show the 2D (x,y) map of the *z*-component of the electron flux $J_z(x,y,z_d) = \Im\{\psi_r^*(x,y,z_d)\partial_z\psi_r(x,y,z_d)\}$ escaping from the π^* resonance and directed perpendicular to the plane of the detector. Here $\Im\{Z\}$ stands for the imaginary part of the complex number *Z*. Because of the projected band gap effect J_z is nearly zero at $x = 0, y = 0$ corresponding to the decay along surface normal (the small background

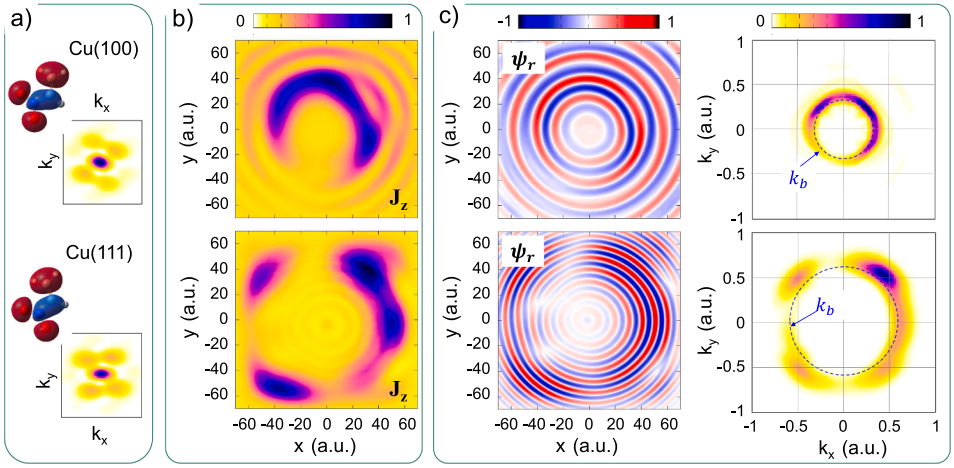

Fig. 4. Analysis of the decay of the nitroethylene anion into the 3D bulk continuum of Cu(1 0 0) – top row, and Cu(1 1 1) – bottom row. Panel (a): top view of the π^* orbital of the nitroethylene molecule calculated in the gas phase using the geometry corresponding to the absorption on the given surface. The interpolated image shows the absolute value of the 2D Fourier transform of the π^* orbital. Panel (b): interpolated image of the $J_z(x,y,z_d)$ – the probability current density component perpendicular to the virtual detector $(x,y,z_d=-30\ \text{a.u.})$-plane located inside the metal at 30 a.u. below the metal surface plane $(x, y, z=0)$ defined by the surface layer of Cu atoms. Results are shown as function of the x-, and y-coordinates. The $(x=0, y=0)$ is set such that the z-axis crosses the middle of the molecular C–N bond. Panel (c) left: interpolated image of the real part of the resonant wave function at the detector plane $\Re\{\psi_r(x,y,z_d)\}$. Panel (c) right: absolute value of the 2D Fourier transform of the $\Re\{\psi_r(x,y,z_d)\}$ shown in panel (b). For Cu(1 0 0) and Cu(1 1 1) the resonance condition $\sqrt{k_x^2+k_y^2}=k_b$ is shown with the dashed blue circle. For further details see the text.

signal is caused by the leakage through the gap into the absorbing potential set at the boundaries of the computational mesh as explained in the Methods section). For both Cu(1 0 0) and Cu(1 1 1) surfaces, J_z maximizes at finite x,y-positions corresponding to the well-defined polar angles θ with respect to the z-axis, and to the well defined azimuthal angles ϕ with respect to the x-axis. Thus, the outgoing electron flux is oriented along several rays originating at the molecule and directed into the metal bulk.

The highly anisotropic character of the decay can be further evidenced with the analysis of the wave function $\psi_r(x,y,z_d)$ of the π^* resonance in the asymptotic region inside metal. In Fig. 4c we show the real part of the resonant wave function in the (x,y)-plane of the detector, $\Re\{\psi_r(x,y,z_d)\}$, and its 2D plane wave decomposition. Here $\Re\{Z\}$ stands for the real part of the complex number Z. The (k_x,k_y) spectrum of the $\Re\{\psi_r(x,y,z_d)\}$ reveals the parallel to the surface momentum of the metal continuum states preferentially populated by the decay of the molecule-localized resonance. As follows from our results for the Cu(1 0 0) and Cu (1 1 1) surfaces, the RET is dominated by the valence band states with $k_{\|}$ slightly above the threshold value given by k_b (see also Fig. 3). Considering the nearly-free electron model of the metal this gives rise to a finite polar angle between the outgoing electron flux and the surface normal $\theta \simeq \arccos(k_b/k)$, where $k=\sqrt{2\left(E_r-E_{VB}^{\Gamma}\right)}$ is the absolute value of the total momentum of the electrons with energy $E\left(\vec{k}\right)=E_r$. In qualitative agreement with the Bardeen's Transfer Hamiltonian Theory, the azimuthal ϕ-angle position of the bright spots on the $k_{\|}=k_b$ circle is associated with the variation of the $|\mathscr{T}|^2$ distribution (see Fig. 4a) along the $k_x=k_b\cos(\phi), k_y=k_b\sin(\phi)$ circle in the (k_x,k_y)-plane.

For the Cu(1 1 1) surface, in addition to the decay into the metal bulk,

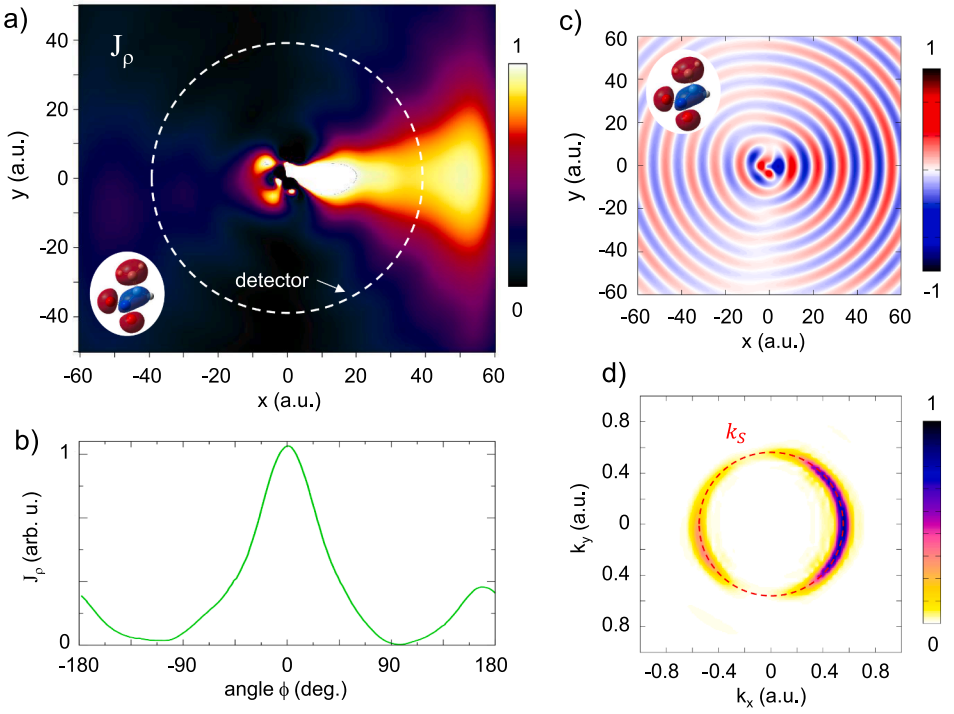

Fig. 5. Analysis of the decay of the nitroethylene anion into the 2D surface state of Cu(1 1 1). Panel (a): interpolated image of the $J_\rho(x,y,z=0)$ – the projection of the probability current density on the radial vector $\vec{\rho}$ of cylindrical (ρ,ϕ,z) coordinates. Results are shown as a function of the x-, and y-coordinates in the Cu(1 1 1) surface plane,$(x,y,z=0)$, defined by the surface layer of Cu atoms. The $(x=0, y=0)$ is set such that the z-axis crosses the middle of the molecular C–N bond. The insert shows the top view of the π^* orbital of nitroethylene calculated in the gas phase for the molecular geometry corresponding to the absorption on Cu(1 1 1) surface. Panel (b): ϕ-angle dependence of the probability current density J_ρ through the circular detector of radius $R_d=40$ a.u.. Position of the detector is sketched by the dashed line. Panel (c): interpolated image of the real part of the resonant wave function $\Re\{\psi_r(x,y,z=0)\}$ in the Cu(1 1 1) surface plane. Panel (d): absolute value of the 2D Fourier transform of the $\Re\{\psi_r(x,y,z=Z_s)\}$. The dashed red circle correspond to the resonance condition $\sqrt{k_x^2+k_y^2}=k_S$ (see Fig. 3).

a decay of the molecular π^* resonance into the electronic states of the 2D surface state continuum with $k_{\parallel} = k_S$ is possible [49,52]. Because the wave function of the surface state is exponentially small in the metal bulk, this decay channel does not clearly appear in the results reported in Fig. 4. The decay into the 2D surface state continuum is evidenced and analysed in Fig. 5 using the wave function of the π^* resonance calculated with WPP in the Cu(1 1 1) surface plane. In Fig. 5a we show the radial ρ component of the probability current density, $J_\rho(x,y,z = 0)$, where the $(x,y,z = 0)$-plane corresponds to the surface layer of Cu atoms. The z-axis of the cylindrical (ρ,ϕ,z) coordinates passes through the center of adsorbed molecule. The WPP results evidence the electron flux leaving the molecule-localized resonance parallel to the surface in the positive direction of the x–axis. We tentatively ascribe the directionality of the decay into the surface state continuum to the shape of the wave function of the π^*-orbital (see the insert). It has a structure of the mode of the cavity open from one side that determines the direction of the electron decay. Note that the molecule localized state decay into the 2D surface state continuum can not be described with the Transfer Hamiltonian Theory applicable for the electron tunneling into the bulk.

Placing a circular detector with radius $\rho_d = 40$ a.u. around the molecule allows to determine the azimuthal ϕ-angle dependence of the outgoing electron flux in the asymptotic region, $J_\rho(\rho_d,\phi,z = 0)$ shown in Fig. 5b. It is characterized by a prominent maximum at $\phi \simeq 0$ with a secondary peak in the opposite $\phi \simeq 180^\circ$ direction. The plane wave decomposition of the resonant wave function in the surface plane (Fig. 5c,d) confirms the highly directional character of the molecular anion decay into the surface state continuum, dominated by the continuum states propagating within narrow angular range around the x-axis. The populated $\overrightarrow{k}_{\parallel}$ states perfectly reside on the k_S circle. At this point it is important to stress that, as follows from the WPP results, the Cu(1 1 1) surface state continuum dominates the decay of the excited π^* resonance. Qualitatively this also can be deduced from the side view of the electron density associated with the quasi-stationary state shown in Fig. 2 for Cu(1 1 1).

In closing this section some remarks are in order concerning the link with previous works. The dominant role of the surface state continuum as well as the blocking effect of the projected band gap have been reported for RET involving excited states of alkali adatoms, as well as for the electron loss by negative ion projectiles interacting with Cu surfaces [49–53]. The high polarizability of the alkali adatoms leads to the formation of a long-lived hybridized state pointing outwards from the metal surface. This long-lived hybridized state is absent for the molecular adsorbates addressed in this work, for which we have found states with very short life-time ($\sim$ 1 fs). Importantly, the molecule–metal interface leads to a very singular azimuthal dependence of the hot electron distribution in the metal not observed for individual atomic adsorbates on metal surfaces. We also stress here that while the method can be applied to extended orbitals, such as π^* orbitals of big planar molecules, special care is needed if the molecule contains conical intersections. In this situation, approaches beyond the adiabatic approximation used here could be required.

3. Conclusions and outlook

In conclusion, we study the dynamics of the excited electronic states localized on organic molecules adsorbed on noble metal surfaces. To this end a 3D description of the system is employed. It is based on an *ab initio* quantum chemistry description of the molecular chemisorption region, and on a model representation of the electron-metal interaction in the asymptotic region. The WPP approach is then used to obtain the time-evolution of the wave function of the active electron involved in the energy conserving transitions between the π^* molecular orbital and the continuum of propagating electronic states of the substrate. The computational strategy adopted here allowed to reveal how the adsorbate–substrate electron transfer depends on the molecular structure, and on the peculiarities of the band structure of the substrate such as the projected band gap and the surface state continuum.

While the study has been performed for the π^* resonance of the nitroethylene molecular anion adsorbed on Cu(1 0 0) and Cu(1 1 1) surfaces, our results ground on robust underlying physics and are thus of general character. Indeed, the ($\sim$1 fs) lifetime of the molecular resonance points at extremely efficient RET between the molecule-localized orbital and the electronic states of the metal continuum, inline with experimental data on adsorbed molecules [29,43,83].

The projected band gap, in the surface electronic structure, and the shape of the molecular localized excited state at the molecule/metal interface, determine the spatial anisotropy of the decay that can be understood on the basis of the perturbation theory [77]. In particular, the decay of the molecule-localized quasi-stationary state leads to hot electrons in the substrate moving at well defined polar and azimuthal angles along several rays. This pronounced anisotropy of the momentum distribution of the hot electrons injected into the substrate by the decaying molecular π^* resonance is the main difference between the present results and earlier data obtained for atomic adsorbates [49].

When present, as in the Cu(1 1 1) surface, the 2D continuum of the surface-localized-state dominates the π^*–orbital/metal coupling and it is the preferential decay channel of the molecular resonance. Similar to the decay into the metal bulk, a high directionality in the decay of the molecule-localized state into the surface state continuum is obtained.

In a more general context, this finding points at strong anisotropy of electron scattering by metal-adsorbed molecules and might have interesting implications for many phenomena linked with molecular adsorption at surfaces. Thus, the surface electronic structure and confinement of the surface state by molecular networks [58–64,84–87], as well as molecular layer induced states [54–57,88–91] might show marked anisotropy depending on the adsorption direction at the surface. When present, anisotropy of adsorbate–adsorbate interactions via the surface state continuum [60,92–98] is also of importance for molecular self-assembly at surfaces. This is without mentioning an eventual possibility of using e.g. photon excitation of the ordered layer of adsorbed molecules to create well directed flow of electrons along the surface.

We hope that the results reported in this work will stimulate further experimental and theoretical studies with perspective to engineer the dynamics of excited electronic states induced at metal surfaces by adsorbed molecules and molecular networks.

4. Methods

4.1. Geometry and electronic structure

The electronic structure and geometry optimization calculations were carried out in the frame of the Density Functional Theory imposing Periodic Boundary Conditions (PBC), to describe in a correct way the metallic character of the surface, using the Vienna Ab initio Simulation Package (VASP) code [99,100]. We choose the optPBE functional [101–104], since it has been shown to provide accurate results for the interaction of organic molecules with metallic surfaces (see e.g. [65,66,105–107]). Interactions between electrons and nuclei were described with the Projector Augmented Wave (PAW) pseudopotentials from the VASP database [108,109]. Electron density was expanded in a plane-wave basis with a cutoff kinetic energy of 500 eV. We have imposed a convergence criteria of 10^{-5} eV for electronic energies in the self-consistent-field cycles, and 10^{-2} eV/Å for the forces in the degrees of freedom that we allowed to relax (x,y,z coordinates of the atoms in the molecule and z coordinate of the atoms in the outermost metal layer).

These optimizations were carried out using a super cell with 5×5 Cu atoms in each direction for the Cu(1 0 0) surface. In the case of Cu(1 1 1) we have used an orthogonal lattice and a similar cell size is obtained with a slab with 5×6 atoms per layer. In order to properly describe the

surface-molecule charge transfer upon adsorption, we have considered a slab with four atomic layers for both surfaces. Since the electron rearrangement is localized close to the surface (see [65,66,110]), increasing the number of layers to compute the change in the potential will not affect the results.

Molecule–metal charge transfer was studied by analyzing the change in the spatial redistribution of the electronic density upon adsorption, which is defined as:

$$\Delta\rho = \rho_{molecule/surface} - \left(\rho_{molecule} + \rho_{surface}\right) \tag{1}$$

where $\rho_{molecule/surface}$ is the electronic density of the whole system, and $\rho_{molecule}$ and $\rho_{surface}$ are the electronic densities of the molecule and surface computed keeping the adsorption geometry.

4.2. Wave packet propagation

The detailed description of the wave packet propagation approach (WPP) used to study the excited electron dynamics has been presented elsewhere [110]. In brief, the time-dependent Schrödinger equation for the electron active in the RET between the molecule and the surface

$$i\partial_t \Psi(\vec{r},t) = \left(-\frac{1}{2}\Delta + V(\vec{r})\right)\Psi(\vec{r},t), \tag{2}$$

is solved in real time with the wave function representation on a 3D equidistant mesh in cartesian coordinates. The initial conditions $\Psi(\vec{r},t=0) \equiv \Psi_0(\vec{r})$ are discussed below. Short-time propagation using the split-operator technique [111,112] is employed along with the pseudospectral Fourier-grid approach [111,113,114]. In the embedding region around the molecule, the 3D potential $V(\vec{r})$ created by the interacting molecule/metal system is obtained from *ab initio* quantum chemistry calculations, and it contains local and nonlocal parts. In the asymptotic region far from the molecule the potential $V(\vec{r})$ is solely given by the electron-metal interaction, which is represented with a 1D model potential function of the z-coordinate perpendicular to the surface [74]. Despite its simplicity this potential captures all the essential characteristics of the surface-projected band structure of the substrate, and therefore it has been widely used for the studies of the dynamics of electronic excitations in metal bulk and at surfaces providing quantitative agreement with experimental data [20,49,57,70,115]. In order to impose the outgoing wave boundary conditions, consistent with calculation of the dynamics of decaying states, the complex absorbing potentials [116,117] (CAPs) are introduced at the boundaries of the mesh. The role of CAPs is to progressively absorb the electron wave packet arriving at the boundaries of the mesh with negligible reflections. In this situation, the time-dependent wave function in the internal (absorption free) region is equivalent to what would be obtained using infinite computational box.

A cubic box with $n_x = n_y = n_z = 1024$ mesh points was used for all the surfaces. In the Cu(1 0 0) and *jellium* surfaces, points were placed with a constant separation of $\Delta x = \Delta y = \Delta z = 0.169$ a.u., while for Cu (1 1 1), $\Delta x = \Delta y = \Delta z = 0.152$ a.u. A time step (Δt) of 0.018 a.u. was employed in all the simulations, ensuring convergence of the split-operator scheme (stability was checked for Δt=0.020 a.u.). A complex absorbing potential with a quadratic form [117] was introduced in the three directions of the box:

$$V_{abs}(\vec{r}) = V_{abs}(x) + V_{abs}(y) + V_{abs}(z), \tag{3}$$

where

$$V_{abs}(\xi) = \begin{cases} -i\lambda_-(\xi-\xi_-)^2 & \text{if } \xi \leqslant \xi_-, \\ -i\lambda_+(\xi-\xi_+)^2 & \text{if } \xi_+ \leqslant \xi, \\ 0 & \text{otherwise.} \end{cases} \tag{4}$$

The following values of the parameters in the optical potential were used: strength $\lambda_- = \lambda_+ = \lambda = 2{\cdot}10^{-4}$ a.u. In each coordinate the $\xi_- < \xi_+$ are set such that the size of the absorption region from the borders of the mesh to the closest onset $\xi_{\{+/-\}}$ points is 30~a.u. at the negative and positive x- and y-coordinates, 20~a.u. at positive z in vacuum, and 35~a.u. at negative z inside metal; $x_+ = y_+ = x_- = y_- = 30$ a.u., $z_- = 35$ a.u. and $z_+ = 20$ a.u.

Using the optimized geometries, the molecular part of the potential for the WPP simulations was obtained with the Abinit package [118], which also takes advantage of the periodic boundary conditions (PBC) in order to have a correct description of the metal surface. The Abinit package allows to describe the interaction between the ionic cores and electrons using the Norm-Conserving pseudopotentials [119], which is mandatory for the WPP technique (see [110] for further details). Plane waves expanded up to a kinetic energy of 32 atomic units were used as basis set to describe the electron density. Electronic energy was converged until an energy difference of 10^{-9} a.u. was reached. Γ point was used to sample the reciprocal space. Since, according to the Koopman's theorem, the LUMO state (Lowest Unoccupied Molecular Orbital) accommodates the extra electron in the molecular anion, we apply the energy correction explained in [110]. Basically, it consists in using molecular projectors to correct the energy of the relevant orbitals. The molecular affinities, computed in the gas phase and needed to determine the orbital energy correction, were obtained with the Gaussian09 [120] package by performing single-point calculations at the CCSD/cc-pVTZ level of theory. The same atomic arrangement as in the adsorbed molecule was considered. In this case the molecular projector was applied to the π^* molecular orbital, since we are dealing with RET from this state. We obtained a U shifting parameter of 3.527 eV for the Cu (1 0 0) and the *jellium* surface, since we used the adsorption geometry of the Cu(1 0 0) to build the *jellium* model, and 3.454 eV for the Cu(1 1 1) surface. The slightly different value in Cu(1 1 1) arises from the small change in the orbital energy due to the different molecular geometry on this substrate.

We extract the energy, E_r, and width, Γ_r, of the decaying states from the autocorrelation function, $\mathscr{A}(t)$, defined as

$$\mathscr{A}(t) = \int \Psi_0^*(\vec{r})\Psi(\vec{r},t)d^3\vec{r}, \tag{5}$$

where $\Psi_0^*(\vec{r})$ stands for the complex conjugate of the initial wave function. As an initial wave function for the WPP we used the LUMO orbital of the molecule in the gas phase. The time-to-energy Fourier transform of $\mathscr{A}(t)$ gives the density of states projected on the initial wave function pDOS [49]:

$$n(E) = \frac{1}{\pi} Re\left\{\int_0^\infty \mathscr{A}(t)e^{iEt}dt\right\} = \sum_k |\langle\varphi_k|\Psi_0\rangle|^2\delta(E_k - E), \tag{6}$$

where $\varphi_k(\vec{r})$ are the eigenstates (continuum and bound) of the Hamiltonian, $\widehat{H} = -\frac{1}{2}\Delta + V(\vec{r})$, of the system. The quasi-stationary molecule-localized decaying states appear as Lorentzian resonances in pDOS allowing extraction of their energy and width (see [110] for details).

4.3. Transfer hamiltonian theory

Within the Transfer Hamiltonian Theory the RET rate between the molecule-localized state and electronic continuum of the model metal surface (*jellium*, or 1D periodic [74]) is given by [77–79]

$$\Gamma = 2\pi\Sigma_{\vec{k}_\parallel}\left|\mathscr{T}_{\vec{k}_\parallel,E_r}\right|^2, \tag{7}$$

where $\vec{k}_\parallel = (k_x, k_y)$, and $\mathscr{T}_{\vec{k}_\parallel,E_r}$ is the transition matrix element between the localized molecular π^* orbital with wave function $\Phi(\vec{r})$ and energy E_r, and the metal continuum state $\psi_{\vec{k}_\parallel,E}(\vec{r})$ defined by its total

energy E and momentum parallel to the surface $\vec{k}_{\parallel}$. The on-energy-shell transitions with $E_r = E$ are considered; Thus, each element is computed as:

$$\mathscr{T}_{\vec{k}_{\parallel},E_r} = \frac{1}{2}\int dx \int dy \left[\psi_{\vec{k}_{\parallel},E_r}(\vec{r})\frac{\partial}{\partial z}\Phi(\vec{r})^{*} - \Phi(\vec{r})^{*}\frac{\partial}{\partial z}\psi_{\vec{k}_{\parallel},E_r}(\vec{r})\right]. \tag{8}$$

The integration runs over the surface parallel to the metal and located at any $z = z_0$ position within the tunneling barrier. The wave functions of the metal continuum states are given by

$$\psi_{\vec{k}_{\parallel},E_r}(\vec{r}) = \frac{1}{2\pi}e^{i\left(k_x x + k_y y\right)}\psi_{\vec{k}_{\parallel},E_r}(z). \tag{9}$$

From Eq. (8) and Eq. (9) it follows that the $\vec{k}_{\parallel}$ dependence of the $\mathscr{T}_{\vec{k}_{\parallel},E_r}$ reflects the 2D plane wave decomposition $\mathscr{F}(k_x,k_y,z_0)$ of the molecular orbital in the (x,y) plane parallel to the surface and located at z_0.

$$\mathscr{F}\left(k_x,k_y,z_0\right) = \frac{1}{2\pi}\int\int dxdy e^{-i\left(k_x x + k_y y\right)}\Phi\left(x,y,z_0\right). \tag{10}$$

For the fixed $k_{\parallel} = k_b$, introducing azimuthal angle ϕ ($k_x = k_b\cos(\phi)$, $k_y = k_b\sin(\phi)$) leads to

$$\mathscr{F}\left(k_b,\phi,z_0\right) = \frac{1}{2\pi}\int\int dxdy e^{-ik_b[x\cos(\phi)+y\sin(\phi)]}\Phi\left(x,y,z_0\right). \tag{11}$$

Declaration of Competing Interest

The authors declare that they have no known competing financial interests or personal relationships that could have appeared to influence the work reported in this paper.

Acknowledgement

We acknowledge the generous allocation of computer time at the Centro de Computación Científica at the Universidad Autónoma de Madrid (CCC-UAM). This work was partially supported by the MICINN - Spanish Ministry of Science and Innovation - projects CTQ2016-76061-P and PID2019-110091 GB-I00, and the 'María de Maeztu' (CEX2018-000805-M) Program for Centers of Excellence in R&D. F.A.G. gratefully acknowledges the hospitality extended to him during his stay at the Institut des Sciences Moléculaires d'Orsay (France).

References

[1] D.J. Wineland, Nobel lecture: Superposition, entanglement, and raising schrödinger's cat, Rev. Mod. Phys. 85 (2013) 1103–1114, https://doi.org/10.1103/RevModPhys.85.1103. URL https://link.aps.org/doi/10.1103/RevModPhys.85.1103.

[2] S. Haroche, Controlling photons in a box and exploring the quantum to classical boundary (nobel lecture), Angew. Chem. Int. Ed. 52 (2013) 10158–10178, https://doi.org/10.1002/anie.201302971.

[3] C. Weitenberg, M. Endres, J.F. Sherson, M. Cheneau, P. Schauss, T. Fukuhara, I. Bloch, S. Kuhr, Single-spin addressing in an atomic mott insulator, Nature 471 (2011) 319–324, https://doi.org/10.1038/nature09827.

[4] J.F. Sherson, C. Weitenberg, M. Endres, M. Cheneau, I. Bloch, S. Kuhr, Single-atom-resolved fluorescence imaging of an atomic mott insulator, Nature 467 (2010) 68–72, https://doi.org/10.1038/nature09378.

[5] C. Monroe, J. Kim, Scaling the ion trap quantum processor, Science 339 (6124) (2013) 1164–1169, https://doi.org/10.1126/science.1231298, arXiv:https://science.sciencemag.org/content/339/6124/1164.full.pdf, URL https://science.sciencemag.org/content/339/6124/1164.

[6] M. Endres, H. Bernien, A. Keesling, H. Levine, E.R. Anschuetz, A. Krajenbrink, C. Senko, V. Vuletic, M. Greiner, M.D. Lukin, Atom-by-atom assembly of defect-free one-dimensional cold atom arrays, Science 354 (6315) (2016) 1024–1027, https://doi.org/10.1126/science.aah3752, arXiv:https://science.sciencemag.org/content/354/6315/1024.full.pdf, URL https://science.sciencemag.org/content/354/6315/1024.

[7] G. Binnig, H. Rohrer, C. Gerber, E. Weibel, Surface studies by scanning tunneling microscopy, Phys. Rev. Lett. 49 (1982) 57–61, https://doi.org/10.1103/PhysRevLett.49.57. URL https://link.aps.org/doi/10.1103/PhysRevLett.49.57.

[8] G. Binnig, H. Rohrer, Scanning tunneling microscopy—from birth to adolescence (nobel lecture), Angew. Chem. Int. Edit. 26 (7) (1987) 606–614, https://doi.org/10.1002/anie.198706061, arXiv:https://onlinelibrary.wiley.com/doi/pdf/10.1002/anie.198706061, URL https://onlinelibrary.wiley.com/doi/abs/10.1002/anie.198706061.

[9] J. Repp, G. Meyer, S.M. Stojkovi, A. Gourdon, C. Joachim, Molecules on insulating films: Scanning-tunneling microscopy imaging of individual molecular orbitals, Phys. Rev. Lett. 94 (2005) 026803, https://doi.org/10.1103/PhysRevLett.94.026803. URL https://link.aps.org/doi/10.1103/PhysRevLett.94.026803.

[10] L. Gross, N. Moll, F. Mohn, A. Curioni, G. Meyer, F. Hanke, M. Persson, High-resolution molecular orbital imaging using a p-wave stm tip, Phys. Rev. Lett. 107 (2011) 086101, https://doi.org/10.1103/PhysRevLett.107.086101. URL https://link.aps.org/doi/10.1103/PhysRevLett.107.086101.

[11] J. Repp, W. Steurer, I. Scivetti, M. Persson, L. Gross, G. Meyer, Charge-state-dependent Diffusion of Individual Gold Adatoms on Ionic Thin NaCl Films, Phys. Rev. Lett. 117 (2016) 146102, https://doi.org/10.1103/PhysRevLett.117.146102. URL https://link.aps.org/doi/10.1103/PhysRevLett.117.146102.

[12] S. Fatayer, B. Schuler, W. Steurer, I. Scivetti, J. Repp, L. Gross, M. Persson, G. Meyer, Reorganization energy upon charging a single molecule on an insulator measured by atomic force microscopy, Nat. Nanotechnol. 13 (2018) 376–380, https://doi.org/10.1038/s41565-018-0087-1.

[13] J. Repp, G. Meyer, S. Paavilainen, F.E. Olsson, M. Persson, Imaging bond formation between a gold atom and pentacene on an insulating surface, Science 312 (5777) (2006) 1196–1199. arXiv:https://science.sciencemag.org/content/312/5777/1196.full.pdf, doi:10.1126/science.1126073. https://science.sciencemag.org/content/312/5777/1196.

[14] C.R. Ast, B. Jäck, J. Senkpiel, M. Eltschka, M. Etzkorn, J. Ankerhold, K. Kern, Sensing the quantum limit in scanning tunnelling spectroscopy, Nat. Commun. 7 (2016) 13009, https://doi.org/10.1038/ncomms13009.

[15] A.L. Vázquez de Parga, R. Miranda, Scanning Tunneling Spectroscopy, Springer, Netherlands, Dordrecht, 2012, pp. 2313–2321, https://doi.org/10.1007/978-90-481-9751-4_111.

[16] H. Ueba, B. Gumhalter, Theory of two-photon photoemission spectroscopy of surfaces, Prog. Surf. Sci. 82 (4) (2007) 193–223, https://doi.org/10.1016/j.progsurf.2007.03.002, part of special issue – Dynamics of Electron Transfer Processes at Surfaces. http://www.sciencedirect.com/science/article/pii/S0079681607000147.

[17] J. Güdde, U. Höfer, Femtosecond time-resolved studies of image-potential states at surfaces and interfaces of rare-gas adlayers, Prog. Surf. Sci. 80 (3) (2005) 49–91, https://doi.org/10.1016/j.progsurf.2005.10.003. URL http://www.sciencedirect.com/science/article/pii/S0079681605000560.

[18] J. Güdde, W. Berthold, U. Höfer, Dynamics of electronic transfer processes at metal/insulator interfaces, Chem. Rev. 106 (10) (2006) 4261–4280, https://doi.org/10.1021/cr050171s.

[19] M. Weinelt, Time-resolved two-photon photoemission from metal surfaces, J. Phys. Condens. Mat. 14 (43) (2002) R1099–R1141, https://doi.org/10.1088/0953-8984/14/43/202.

[20] X.-Y. Zhu, Electron transfer at molecule-metal interfaces: A two-photon photoemission study, Annu. Rev. Phys. Chem. 53 (1) (2002) 221–247. arXiv:https://doi.org/10.1146/annurev.physchem.53.082801.093725, doi:10.1146/annurev.physchem.53.082801.093725.

[21] A. Ebner, L. Wildling, H. Gruber, Functionalization of AFM Tips and Supports for Molecular Recognition Force Spectroscopy and Recognition Imaging, in: N. Santos, F. Carvalho (Eds.), Atomic Force Microscopy. Methods in Molecular Biology, vol. 1886, Humana Press, New York, NY, 2018. doi:10.1007/978-1-4939-8894-5_7.

[22] F. Mohn, L. Gross, N. Moll, G. Meyer, Imaging the charge distribution within a single molecule, Nat. Nanotechnol. 7 (2012) 227–231, https://doi.org/10.1038/nnano.2012.20.

[23] L. Gross, F. Mohn, N. Moll, B. Schuler, A. Criado, E. Guitián, D. Peña, A. Gourdon, G. Meyer, Bond-order discrimination by atomic force microscopy, Science 337 (6100) (2012) 1326–1329, https://doi.org/10.1126/science.1225621, arXiv:https://science.sciencemag.org/content/337/6100/1326.full.pdf, URL https://science.sciencemag.org/content/337/6100/1326.

[24] B. Schuler, W. Liu, A. Tkatchenko, N. Moll, G. Meyer, A. Mistry, D. Fox, L. Gross, Adsorption geometry determination of single molecules by atomic force microscopy, Phys. Rev. Lett. 111 (2013) 106103, https://doi.org/10.1103/PhysRevLett.111.106103.

[25] B.C. Stipe, M.A. Rezaei, W. Ho, Single-molecule vibrational spectroscopy and microscopy, Science 280 (5370) (1998) 1732–1735, https://doi.org/10.1126/science.280.5370.1732, arXiv:http://www.sciencemag.org/content/280/5370/1732.full.pdf, URL http://www.sciencemag.org/content/280/5370/1732.abstract.

[26] L.J. Lauhon, W. Ho, Single-Molecule Chemistry and Vibrational Spectroscopy: Pyridine and Benzene on Cu(001), J. Phys. Chem. A 104 (11) (2000) 2463–2467, https://doi.org/10.1021/jp991768c.

[27] X.H. Qiu, G.V. Nazin, W. Ho, Vibrationally resolved fluorescence excited with submolecular precision, Science 299 (5606) (2003) 542–546, https://doi.org/10.1126/science.1078675, arXiv:https://science.sciencemag.org/content/299/5606/542.full.pdf, URL https://science.sciencemag.org/content/299/5606/542.

[28] A. Safiei, J. Henzl, K. Morgenstern, Isomerization of an azobenzene derivative on a thin insulating layer by inelastically tunneling electrons, Phys. Rev. Lett. 104 (2010) 216102, https://doi.org/10.1103/PhysRevLett.104.216102.

[29] J. Schaffert, M.C. Cottin, A. Sonntag, H. Karacuban, C.A. Bobisch, N. Lorente, J.-P. Gauyacq, R. Möller, Imaging the dynamics of individually adsorbed molecules, Nat. Mater. 12 (2013) 223–227, https://doi.org/10.1038/nmat3527.

[30] S.-W. Hla, K.-H. Rieder, Stm control of chemical reactions: Single-molecule synthesis, Annu. Rev. Phys. Chem. 54 (1) (2003) 307–330, https://doi.org/10.1146/annurev.physchem.54.011002.103852.

[31] P. Liljeroth, J. Repp, G. Meyer, Current-induced hydrogen tautomerization and conductance switching of naphthalocyanine molecules, Science 317 (5842) (2007) 1203–1206, https://doi.org/10.1126/science.1144366, arXiv:https://science.sciencemag.org/content/317/5842/1203.full.pdf, URL https://science.sciencemag.org/content/317/5842/1203.

[32] T. Kumagai, J.N. Ladenthin, Y. Litman, M. Rossi, L. Grill, S. Gawinkowski, J. Waluk, M. Persson, Quantum tunneling in real space: Tautomerization of single porphycene molecules on the (111) surface of cu, ag, and au, J. Chem. Phys. 148 (10) (2018) 102330, https://doi.org/10.1063/1.5004602.

[33] K. Kaiser, L. Gross, F. Schulz, A single-molecule chemical reaction studied by high-resolution atomic force microscopy and scanning tunneling microscopy induced light emission, ACS Nano 13 (6) (2019) 6947–6954, https://doi.org/10.1021/acsnano.9b01852.

[34] G. Reecht, F. Scheurer, V. Speisser, Y.J. Dappe, F. Mathevet, G. Schull, Electroluminescence of a polythiophene molecular wire suspended between a metallic surface and the tip of a scanning tunneling microscope, Phys. Rev. Lett. 112 (2014) 047403, https://doi.org/10.1103/PhysRevLett.112.047403.

[35] B. Doppagne, M.C. Chong, E. Lorchat, S. Berciaud, M. Romeo, H. Bulou, A. Boeglin, F. Scheurer, G. Schull, Vibronic spectroscopy with submolecular resolution from stm-induced electroluminescence, Phys. Rev. Lett. 118 (2017) 127401, https://doi.org/10.1103/PhysRevLett.118.127401.

[36] J. Kroger, B. Doppagne, F. Scheurer, G. Schull, Fano description of single-hydrocarbon fluorescence excited by a scanning tunneling microscope, Nano Lett. 18 (6) (2018) 3407–3413, https://doi.org/10.1021/acs.nanolett.8b00304.

[37] B. Doppagne, M.C. Chong, H. Bulou, A. Boeglin, F. Scheurer, G. Schull, Electrofluorochromism at the single-molecule level, Science 361 (6399) (2018) 251–255, https://doi.org/10.1126/science.aat1603, arXiv:http://science.sciencemag.org/content/361/6399/251.full.pdf, http://science.sciencemag.org/content/361/6399/251.

[38] D. Pommier, R. Bretel, L.E.P. López, F. Fabre, A. Mayne, E. Boer-Duchemin, G. Dujardin, G. Schull, S. Berciaud, E. Le Moal, Scanning tunneling microscope-induced excitonic luminescence of a two-dimensional semiconductor, Phys. Rev. Lett. 123 (2019) 027402, https://doi.org/10.1103/PhysRevLett.123.027402.

[39] H. Guo, P. Saalfrank, T. Seideman, Theory of photoinduced surface reactions of admolecules, Prog. Surf. Sci. 62 (7) (1999) 239–303, https://doi.org/10.1016/S0079-6816(99)00013-1, http://www.sciencedirect.com/science/article/pii/S0079681699000131.

[40] J.C. Tully, Chemical dynamics at metal surfaces, Annu. Rev. Phys. Chem. 51 (1) (2000) 153–178, https://doi.org/10.1146/annurev.physchem.51.1.153.

[41] P. Saalfrank, Quantum dynamical approach to ultrafast molecular desorption from surfaces, Chem. Rev. 106 (10) (2006) 4116–4159, https://doi.org/10.1021/cr0501691.

[42] K.R. Rusimova, R.M. Purkiss, R. Howes, F. Lee, S. Crampin, P.A. Sloan, Regulating the femtosecond excited-state lifetime of a single molecule, Science 361 (6406) (2018) 1012–1016, https://doi.org/10.1126/science.aat9688, arXiv:http://science.sciencemag.org/content/361/6406/1012.full.pdf, URL http://science.sciencemag.org/content/361/6406/1012.

[43] H. Petek, Photoexcitation of adsorbates on metal surfaces: One-step or three-step, J. Chem. Phys. 137 (9) (2012) 091704, https://doi.org/10.1063/1.4746801.

[44] K. Shimizu, R. Payling, H. Habazaki, P. Skeldon, G.E. Thompson, Rf-gdoes depth profiling analysis of a monolayer of thiourea adsorbed on copper, J. Anal. At. Spectrom. 19 (2004) 692–695, https://doi.org/10.1039/B400918P.

[45] I.S. Molchan, G.E. Thompson, P. Skeldon, A. Licciardello, N. Tuccitto, A. Tempez, Analysis of molecular monolayers adsorbed on metal surfaces by glow discharge optical emission spectrometry, J. Anal. At. Spectrom. 28 (2013) 121–126, https://doi.org/10.1039/C2JA30247K.

[46] Y. Sano, I. Kawayama, M. Tabata, K.A. Salek, H. Murakami, M. Wang, R. Vajtai, P. M. Ajayan, J. Kono, M. Tonouchi, Imaging molecular adsorption and desorption dynamics on graphene using terahertz emission spectroscopy, Sci. Rep. 4 (1) (2014) 6046, https://doi.org/10.1038/srep06046.

[47] A. Stiebeiner, O. Rehband, R. Garcia-Fernandez, A. Rauschenbeutel, Ultra-sensitive fluorescence spectroscopy of isolated surface-adsorbed molecules using an optical nanofiber, Opt. Express 17 (24) (2009) 21704–21711, https://doi.org/10.1364/OE.17.021704. URL http://www.opticsexpress.org/abstract.cfm?URI=oe-17-24-21704.

[48] C.D. Lindstrom, X.-Y. Zhu, Photoinduced electron transfer at molecule metal interfaces, Chem. Rev. 106 (10) (2006) 4281–4300, https://doi.org/10.1021/cr0501689.

[49] E.V. Chulkov, A.G. Borisov, J.P. Gauyacq, D. Sánchez-Portal, V.M. Silkin, V. P. Zhukov, P.M. Echenique, Electronic excitations in metals and at metal surfaces, Chem. Rev. 106 (10) (2006) 4160–4206, https://doi.org/10.1021/cr0501660.

[50] M. Bauer, S. Pawlik, M. Aeschlimann, Decay dynamics of photoexcited alkali chemisorbates: Real-time investigations in the femtosecond regime, Phys. Rev. B 60 (1999) 5016–5028, https://doi.org/10.1103/PhysRevB.60.5016. URL https://link.aps.org/doi/10.1103/PhysRevB.60.5016.

[51] H. Petek, M. Weida, H. Nagano, S. Ogawa, Electronic relaxation of alkali metal atoms on the cu(111) surface, Surf. Sci. 451 (1) (2000) 22–30, https://doi.org/10.1016/S0039-6028(00)00004-2.

[52] A.G. Borisov, J.P. Gauyacq, A.K. Kazansky, E.V. Chulkov, V.M. Silkin, P. M. Echenique, Long-lived excited states at surfaces: Cs/Cu(111) and Cs/Cu(100) systems, Phys. Rev. Lett. 86 (2001) 488–491, https://doi.org/10.1103/PhysRevLett.86.488. URL https://link.aps.org/doi/10.1103/PhysRevLett.86.488.

[53] A.G. Borisov, V. Sametoglu, A. Winkelmann, A. Kubo, N. Pontius, J. Zhao, V. M. Silkin, J.P. Gauyacq, E.V. Chulkov, P.M. Echenique, H. Petek, πresonance of chemisorbed alkali atoms on noble metals, Phys. Rev. Lett. 101 (2008) 266801, https://doi.org/10.1103/PhysRevLett.101.266801. URL https://link.aps.org/doi/10.1103/PhysRevLett.101.266801.

[54] D.B. Dougherty, P. Maksymovych, J. Lee, J.T. Yates, Local spectroscopy of image-potential-derived states: From single molecules to monolayers of benzene on cu (111), Phys. Rev. Lett. 97 (2006) 236806, https://doi.org/10.1103/PhysRevLett.97.236806.

[55] C.H. Schwalb, S. Sachs, M. Marks, A. Schöll, F. Reinert, E. Umbach, U. Höfer, Electron lifetime in a shockley-type metal-organic interface state, Phys. Rev. Lett. 101 (2008) 146801, https://doi.org/10.1103/PhysRevLett.101.146801. URL https://link.aps.org/doi/10.1103/PhysRevLett.101.146801.

[56] I. Kröger, B. Stadtmüller, C. Stadler, J. Ziroff, M. Kochler, A. Stahl, F. Pollinger, T.-L. Lee, J. Zegenhagen, F. Reinert, C. Kumpf, Submonolayer growth of copper-phthalocyanine on ag(111), New J. Phys. 12 (8) (2010) 083038, https://doi.org/10.1088/1367-2630/12/8/083038.

[57] S.S. Tsirkin, N.L. Zaitsev, I.A. Nechaev, R. Tonner, U. Höfer, E.V. Chulkov, Inelastic decay of electrons in shockley-type metal-organic interface states, Phys. Rev. B 92 (2015) 235434, https://doi.org/10.1103/PhysRevB.92.235434. URL https://link.aps.org/doi/10.1103/PhysRevB.92.235434.

[58] J.V. Barth, Molecular architectonic on metal surfaces, Annu. Rev. Phys. Chem. 58 (1) (2007) 375–407, https://doi.org/10.1146/annurev.physchem.56.092503.141259.

[59] L. Bartels, Tailoring molecular layers at metal surfaces, Nat. Chem. 2 (2010) 87–95, https://doi.org/10.1038/nchem.517.

[60] P. Han, P.S. Weiss, Electronic substrate-mediated interactions, Surf. Sci. Rep. 67 (2) (2012) 19–81, https://doi.org/10.1016/j.surfrep.2011.11.001. URL http://www.sciencedirect.com/science/article/pii/S0167572911000598.

[61] J. Lobo-Checa, M. Matena, K. Müller, J.H. Dil, F. Meier, L.H. Gade, T.A. Jung, M. Stöhr, Band formation from coupled quantum dots formed by a nanoporous network on a copper surface, Science 325 (5938) (2009) 300–303, https://doi.org/10.1126/science.1175141, arXiv:https://science.sciencemag.org/content/325/5938/300.full.pdf, URL https://science.sciencemag.org/content/325/5938/300.

[62] F. Klappenberger, D. Kühne, W. Krenner, I. Silanes, A. Arnau, F.J. García de Abajo, S. Klyatskaya, M. Ruben, J.V. Barth, Tunable quantum dot arrays formed from self-assembled metal-organic networks, Phys. Rev. Lett. 106 (2011) 026802, https://doi.org/10.1103/PhysRevLett.106.026802.

[63] J. Wyrick, D.-H. Kim, D. Sun, Z. Cheng, W. Lu, Y. Zhu, K. Berland, Y.S. Kim, E. Rotenberg, M. Luo, P. Hyldgaard, T.L. Einstein, L. Bartels, Do two-dimensional "noble gas atoms produce molecular honeycombs at a metal surface? Nano Lett. 11 (7) (2011) 2944–2948, https://doi.org/10.1021/nl201441b.

[64] F. Klappenberger, D. Kühne, W. Krenner, I.n. Silanes, A. Arnau, F.J. García de Abajo, S. Klyatskaya, M. Ruben, J.V. Barth, Dichotomous array of chiral quantum corrals by a self-assembled nanoporous kagomé network, Nano Lett. 9 (10) (2009) 3509–3514, https://doi.org/10.1021/nl901700b.

[65] F. Aguilar-Galindo, S. Díaz-Tendero, Theoretical insights into vinyl derivatives adsorption on a cu(100) surface, J. Phys. Chem. C 122 (48) (2018) 27301–27313, https://doi.org/10.1021/acs.jpcc.8b06142.

[66] F. Aguilar-Galindo, S. Díaz-Tendero, Outstanding energy exchange between organic molecules and metal surfaces: Decomposition kinetics of excited vinyl derivatives driven by the interaction with a cu(111) surface, J. Phys. Chem. C 123 (32) (2019) 19625–19636, https://doi.org/10.1021/acs.jpcc.9b04898.

[67] Energy obtained as the difference between the anionic and the neutral species. geometry is optimized at the mp2/cc-pvdz level and a single point energy calculation over this structure is carried out at the ccsd/cc-pvdz level.

[68] J.E. Inglesfield, Surface electronic structure, Rep. Prog. Phys. 45 (3) (1982) 223–284, https://doi.org/10.1088/0034-4885/45/3/001.

[69] A. Ruban, B. Hammer, P. Stoltze, H. Skriver, J. Nørskov, Surface electronic structure and reactivity of transition and noble metals, J. Mol. Catal. A – Chem. 115 (3) (1997) 421–429, https://doi.org/10.1016/S1381-1169(96)00348-2. URL http://www.sciencedirect.com/science/article/pii/S1381116996003482.

[70] P. Echenique, R. Berndt, E. Chulkov, T. Fauster, A. Goldmann, U. Höfer, Decay of electronic excitations at metal surfaces, Surf. Sci. Rep. 52 (7–8) (2004) 219–317, https://doi.org/10.1016/j.surfrep.2004.02.002. URL http://www.sciencedirect.com/science/article/pii/S0167572904000123.

[71] K. Schubert, A. Damm, S.V. Eremeev, M. Marks, M. Shibuta, W. Berthold, J. Güdde, A.G. Borisov, S.S. Tsirkin, E.V. Chulkov, U. Höfer, Momentum-resolved electron dynamics of image-potential states on cu and ag surfaces, Phys. Rev. B 85 (2012) 205431, https://doi.org/10.1103/PhysRevB.85.205431.

[72] J. Goodisman, Thomas–fermi–dirac-jellium model of the metal surface: Change of surface potential with charge, J. Chem. Phys. 86 (2) (1987) 882–886, https://doi.org/10.1063/1.452290.

[73] A. Kiejna, Stabilized jellium–simple model for simple–metal surfaces, Prog. Surf. Sci. 61 (5) (1999) 85–125, https://doi.org/10.1016/S0079-6816(99)00011-8. URL http://www.sciencedirect.com/science/article/pii/S0079681699000118.

[74] E. Chulkov, V. Silkin, P. Echenique, Image potential states on metal surfaces: Binding energies and wavefunctions, Surf. Sci. 437 (3) (1999) 330–352, https://doi.org/10.1016/S0039-6028(99)00668-8. URL http://www.sciencedirect.com/science/article/pii/S0039602899006688.

[75] S. Davison, M. Steslicka, Basic Theory of Surface States, Monographs on the Physics & Ch, Clarendon Press, 1996.

[76] A.G. Borisov, A.K. Kazansky, J.P. Gauyacq, Resonant charge transfer in ion–metal surface collisions: Effect of a projected band gap in the h-Cu(111) system, Phys. Rev. B 59 (1999) 10935–10949, https://doi.org/10.1103/PhysRevB.59.10935. https://link.aps.org/doi/10.1103/PhysRevB.59.10935.

[77] J. Bardeen, Tunnelling from a many-particle point of view, Phys. Rev. Lett. 6 (1961) 57–59, https://doi.org/10.1103/PhysRevLett.6.57.

[78] M.C. Payne, Transfer hamiltonian description of resonant tunnelling, J. Phys. C: Solid State Phys 19 (8) (1986) 1145–1155, https://doi.org/10.1088/0022-3719/19/8/013.

[79] J. Tersoff, D.R. Hamann, Theory of the scanning tunneling microscope, Phys. Rev. B 31 (1985) 805–813, https://doi.org/10.1103/PhysRevB.31.805.

[80] W.A. Hofer, A.S. Foster, A.L. Shluger, Theories of scanning probe microscopes at the atomic scale, Rev. Mod. Phys. 75 (2003) 1287–1331, https://doi.org/10.1103/RevModPhys.75.1287. https://link.aps.org/doi/10.1103/RevModPhys.75.1287.

[81] M. Parzefall, L. Novotny, Optical antennas driven by quantum tunneling: a key issues review, Rep. Prog. Phys. 82 (11) (2019) 112401, https://doi.org/10.1088/1361-6633/ab4239.

[82] F. Evers, R. Korytár, S. Tewari, J.M. van Ruitenbeek, Advances and challenges in single-molecule electron transport, Rev. Mod. Phys. 92 (2020) 035001, https://doi.org/10.1103/RevModPhys.92.035001.

[83] D.P. Woodruff, Characterising Molecules and Molecular Interactions on Surfaces, 3rd ed., Cambridge University Press, 2016, pp. 383–467, https://doi.org/10.1017/CBO9781139149716.009.

[84] P.J. Blowey, B. Sohail, L.A. Rochford, T. Lafosse, D.A. Duncan, P.T.P. Ryan, D. A. Warr, T.-L. Lee, G. Costantini, R.J. Maurer, D.P. Woodruff, Alkali doping leads to charge-transfer salt formation in a two-dimensional metal–organic framework, ACS Nano 14 (6) (2020) 7475–7483, https://doi.org/10.1021/acsnano.0c03133.

[85] O.T. Hofmann, P. Rinke, M. Scheffler, G. Heimel, Integer versus fractional charge transfer at metal(/insulator)/organic interfaces: Cu(/nacl)/tcne, ACS Nano 9 (5) (2015) 5391–5404, https://doi.org/10.1021/acsnano.5b01164.

[86] V.O. Özçelik, Y. Li, W. Xiong, F. Paesani, Modeling spontaneous charge transfer at metal/organic hybrid heterostructures, J. Phys. Chem. C 124 (8) (2020) 4802–4809, https://doi.org/10.1021/acs.jpcc.9b10055.

[87] U. Schlickum, R. Decker, F. Klappenberger, G. Zoppellaro, S. Klyatskaya, M. Ruben, I. Silanes, A. Arnau, K. Kern, H. Brune, J.V. Barth, Metal organic honeycomb nanomeshes with tunable cavity size, Nano Lett. 7 (12) (2007) 3813–3817, https://doi.org/10.1021/nl072466m.

[88] M. Marks, A. Schöll, U. Höfer, Formation of metal-organic interface states studied with 2 ppe, J. Electron. Spectrosc. 195 (2014) 263–271, https://doi.org/10.1016/j.elspec.2014.02.009.

[89] L. Giovanelli, F.C. Bocquet, P. Amsalem, H.-L. Lee, M. Abel, S. Clair, M. Koudia, T. Faury, L. Petaccia, D. Topwal, E. Salomon, T. Angot, A.A. Cafolla, N. Koch, L. Porte, A. Goldoni, J.-M. Themlin, Interpretation of valence band photoemission spectra at organic-metal interfaces, Phys. Rev. B 87 (2013) 035413, https://doi.org/10.1103/PhysRevB.87.035413. URL https://link.aps.org/doi/10.1103/PhysRevB.87.035413.

[90] C. Wang, Y. Li, W. Xiong, Extracting molecular responses from ultrafast charge dynamics at material interfaces, J. Mater. Chem. C 8 (2020) 12062–12067, https://doi.org/10.1039/D0TC01819H.

[91] M. Hollerer, D. Lüftner, P. Hurdax, T. Ules, S. Soubatch, F.S. Tautz, G. Koller, P. Puschnig, M. Sterrer, M.G. Ramsey, Charge transfer and orbital level alignment at inorganic/organic interfaces: The role of dielectric interlayers, ACS Nano 11 (6) (2017) 6252–6260, https://doi.org/10.1021/acsnano.7b02449.

[92] T.B. Grimley, The indirect interaction between atoms or molecules adsorbed on metals, P. Phys. Soc. 90 (3) (1967) 751–764, https://doi.org/10.1088/0370-1328/90/3/320.

[93] T.L. Einstein, Comment on "oscillatory indirect interaction between adsorbed atoms — non-asymptotic behavior in tight-binding models at realistic parameters by k.h. lau and w. kohn, Surf. Sci. 75 (1) (1978) 161–167, https://doi.org/10.1016/0039-6028(78)90062-6. URL http://www.sciencedirect.com/science/article/pii/0039602878900626.

[94] P. Hyldgaard, M. Persson, Long-ranged adsorbate-adsorbate interactions mediated by a surface-state band, J. Phys. Condens. Mat. 12 (1) (1999) L13–L19, https://doi.org/10.1088/0953-8984/12/1/103.

[95] J. Repp, F. Moresco, G. Meyer, K.-H. Rieder, P. Hyldgaard, M. Persson, Substrate mediated long-range oscillatory interaction between adatoms: Cu/cu(111), Phys. Rev. Lett. 85 (2000) 2981–2984, https://doi.org/10.1103/PhysRevLett.85.2981.

[96] F. Silly, M. Pivetta, M. Ternes, F. Patthey, J.P. Pelz, W.-D. Schneider, Creation of an atomic superlattice by immersing metallic adatoms in a two-dimensional electron sea, Phys. Rev. Lett. 92 (2004) 016101, https://doi.org/10.1103/PhysRevLett.92.016101.

[97] T. Yokoyama, T. Takahashi, K. Shinozaki, M. Okamoto, Quantitative analysis of long-range interactions between adsorbed dipolar molecules on cu(111), Phys. Rev. Lett. 98 (2007) 206102, https://doi.org/10.1103/PhysRevLett.98.206102.

[98] Y. Wang, X. Ge, C. Manzano, J. Kröger, R. Berndt, W.A. Hofer, H. Tang, J. Cerda, Supramolecular patterns controlled by electron interference and direct intermolecular interactions, J. Am. Chem. Soc. 131 (30) (2009) 10400–10402, https://doi.org/10.1021/ja903506s.

[99] G. Kresse, J. Furthmühller, Efficiency of ab-initio total energy calculations for metals and semiconductors using a plane-wave basis set, Comput. Mat. Sci. 6 (1996) 15–50.

[100] G. Kresse, J. Furthmühller, Efficient iterative schemes for ab-initio total-energy calculations using a plane-wave basis set, Phys. Rev. B 54 (1996) 11169.

[101] M. Dion, H. Rydberg, E. Schröder, D.C. Langreth, B.I. Lundqvist, Van der Waals Density Functional for General Geometries, Phys. Rev. Lett. 92 (2004) 246401, https://doi.org/10.1103/PhysRevLett.92.246401.

[102] G. Román-Pérez, J.M. Soler, Efficient Implementation of a Van der Waals Density Functional: Application to Double-Wall Carbon Nanotubes, Phys. Rev. Lett. 103 (2009) 096102, https://doi.org/10.1103/PhysRevLett.103.096102.

[103] J. c. v. Klime, D.R. Bowler, A. Michaelides, Chemical Accuracy for the Van der Waals Density Functional, J. Phys.-Condens. Mat. 22 (2) (2010) 022201. URL http://stacks.iop.org/0953-8984/22/i=2/a=022201.

[104] J. c. v. Klime, D.R. Bowler, A. Michaelides, Van der Waals Density Functionals Applied to Solids, Phys. Rev. B 83 (2011) 195131. doi:10.1103/PhysRevB.83.195131. https://link.aps.org/doi/10.1103/PhysRevB.83.195131.

[105] W. Liu, A. Tkatchenko, M. Scheffler, Modeling adsorption and reactions of organic molecules at metal surfaces, Acc. Chem. Res. 47 (11) (2014) 3369–3377. arXiv:https://doi.org/10.1021/ar500118y, doi:10.1021/ar500118y. doi: 10.1021/ar500118y.

[106] J. Björk, S. Stafström, Adsorption of Large Hydrocarbons on Coinage Metals: a Van der Waals Density Functional Study, ChemPhysChem 15 (13) (2014) 2851–2858. arXiv:https://onlinelibrary.wiley.com/doi/pdf/10.1002/cphc.201402063, doi:10.1002/cphc.201402063. https://onlinelibrary.wiley.com/doi/abs/10.1002/cphc.201402063.

[107] S. Gautier, S.N. Steinmann, C. Michel, P. Fleurat-Lessard, P. Sautet, Molecular adsorption at Pt(111). How Accurate Are DFT Functionals? Phys. Chem. Chem. Phys. 17 (2015) 28921–28930, https://doi.org/10.1039/C5CP04534G.

[108] P.E. Blöchl, Projector-augmented wave method, Phys. Rev. B 50 (1994) 17953–17979, https://doi.org/10.1103/PhysRevB.50.17953.

[109] G. Kresse, D. Joubert, From ultrasoft pseudopotentials to the projector augmented-wave method, Phys. Rev. B 59 (1999) 1758–1775, https://doi.org/10.1103/PhysRevB.59.1758.

[110] F. Aguilar-Galindo, A.G. Borisov, S. Díaz-Tendero, Ultrafast dynamics of electronic resonances in molecules adsorbed on metal surfaces: a wave packet propagation approach, J. Chem. Theory Comput. (2021), https://doi.org/10.1021/acs.jctc.0c01031 (accepted).

[111] M. Feit, J. Fleck, A. Steiger, Solution of the Schrödinger Equation by a Spectral Method, J. Comput. Phys. 47 (3) (1982) 412–433, https://doi.org/10.1016/0021-9991(82)90091-2. URL http://www.sciencedirect.com/science/article/pii/0021999182900912.

[112] C. Leforestier, R.H. Bisseling, C. Cerjan, M.D. Feit, R. Friesner, A. Guldberg, A. Hammerich, G. Jolicard, W. Karrlein, H.-D. Meyer, N. Lipkin, O. Roncero, R. Kosloff, A comparison of different propagation schemes for the time dependent schrödinger equation, J. Comput. Phys. 94 (1) (1991) 59–80, https://doi.org/10.1016/0021-9991(91)90137-A.

[113] M.D. Feit, J.A. Fleck, Solution of the schrödinger equation by a spectral method ii: Vibrational energy levels of triatomic molecules, J. Chem. Phys. 78 (1) (1983) 301–308, https://doi.org/10.1063/1.444501.

[114] R. Kosloff, Time-dependent quantum-mechanical methods for molecular dynamics, J. Phys. Chem. 92 (8) (1988) 2087–2100, https://doi.org/10.1021/j100319a003.

[115] P. Echenique, J. Pitarke, E. Chulkov, A. Rubio, Theory of inelastic lifetimes of low-energy electrons in metals, Chem. Phys. 251 (1) (2000) 1–35, https://doi.org/10.1016/S0301-0104(99)00313-4. URL http://www.sciencedirect.com/science/article/pii/S0301010499003134.

[116] D. Neuhauser, M. Baer, The application of wave packets to reactive atom-diatom systems: A new approach, J. Chem. Phys. 91 (8) (1989) 4651–4657, https://doi.org/10.1063/1.456755.

[117] G.-J. Kroes, D. Neuhauser, Avoiding long propagation times in wave packet calculations on scattering with resonances: A hybrid approach involving the lanczos method, J. Chem. Phys. 105 (1996) 9104–9114, https://doi.org/10.1063/1.472744.

[118] X. Gonze, F. Jollet, F. Abreu Araujo, D. Adams, B. Amadon, T. Applencourt, C. Audouze, J.-M. Beuken, J. Bieder, A. Bokhanchuk, E. Bousquet, F. Bruneval, D. Caliste, M. Côté, F. Dahm, F. Da Pieve, M. Delaveau, M. Di Gennaro, B. Dorado, C. Espejo, G. Geneste, L. Genovese, A. Gerossier, M. Giantomassi, Y. Gillet, D. Hamann, L. He, G. Jomard, J. Laflamme Janssen, S. Le Roux, A. Levitt, A. Lherbier, F. Liu, I. Lukacevic, A. Martin, C. Martins, M. Oliveira, S. Poncé, Y. Pouillon, T. Rangel, G.-M. Rignanese, A. Romero, B. Rousseau, O. Rubel, A. Shukri, M. Stankovski, M. Torrent, M. Van Setten, B. Van Troeye, M. Verstraete, D. Waroquiers, J. Wiktor, B. Xu, A. Zhou, J. Zwanziger, Recent developments in the ABINIT software package, Comput. Phys. Commun. 205 (2016) 106–131, https://doi.org/10.1016/j.cpc.2016.04.003.

[119] D.R. Hamann, Optimized Norm-Conserving Vanderbilt Pseudopotentials, Phys. Rev. B 88 (2013) 085117, https://doi.org/10.1103/PhysRevB.88.085117.

[120] M.J. Frisch, G.W. Trucks, H.B. Schlegel, G.E. Scuseria, M.A. Robb, J.R. Cheeseman, G. Scalmani, V. Barone, B. Mennucci, G.A. Petersson, H. Nakatsuji, M. Caricato, X. Li, H.P. Hratchian, A.F. Izmaylov, J. Bloino, G. Zheng, J.L. Sonnenberg, M. Hada, M. Ehara, K. Toyota, R. Fukuda, J. Hasegawa, M. Ishida, T. Nakajima, Y. Honda, O. Kitao, H. Nakai, T. Vreven, J.A. Montgomery, Jr., J.E. Peralta, F. Ogliaro, M. Bearpark, J.J. Heyd, E. Brothers, K.N. Kudin, V.N. Staroverov, R. Kobayashi, J. Normand, K. Raghavachari, A. Rendell, J.C. Burant, S.S. Iyengar, J. Tomasi, M. Cossi, N. Rega, J.M. Millam, M. Klene, J.E. Knox, J.B. Cross, V. Bakken, C. Adamo, J. Jaramillo, R. Gomperts, R.E. Stratmann, O. Yazyev, A.J. Austin, R. Cammi, C. Pomelli, J.W. Ochterski, R.L. Martin, K. Morokuma, V.G. Zakrzewski, G.A. Voth, P. Salvador, J.J. Dannenberg, S. Dapprich, A.D. Daniels, Ö. Farkas, J.B. Foresman, J.V. Ortiz, J. Cioslowski, D.J. Fox, Gaussian 09 Revision E.01, gaussian inc. wallingford ct 2013 (2013).